Dynamics of integrin clustering at focal contacts of endothelial cells studied by multimode imaging microscopy

Keisuke Kawakami[1,2], Hitoshi Tatsumi[1] and Masahiro Sokabe[1,3,*]

[1]Department of Physiology, Nagoya University Graduate School of Medicine, 65 Tsurumai Showa-ku, Nagoya Aichi 4668550, Japan
[2]Department of Physical Therapy, Nagoya University School of Health Sciences, 1-1-20 Daikominami Higashi-ku, Nagoya Aichi 4618673, Japan
[3]ICORP, Cell Mechanosensing Project, Japan Science and Technology Corporation, 65 Tsurumai Showa-ku, Nagoya Aichi 4668550, Japan
*Author for correspondence (e-mail: msokabe@med.nagoya-u.ac.jp)

Accepted 22 May 2001
Journal of Cell Science 114, 3125-3135 (2001) © The Company of Biologists Ltd

SUMMARY

Human umbilical vein endothelial cells were stained with FITC-labeled anti-β_1 integrin antibody and plated on a glass cover slip to elucidate the mechanism of integrin clustering during focal contact formation. The process of integrin clustering was observed by time-lapse total-internal-reflection fluorescence microscopy, which can selectively visualize the labeled integrins at the basal surface of living cells. The clustering of integrins at focal contacts started at 1 hour after plating and individual clusters kept growing for ~6 hours. Most integrin clusters (~80%) elongated towards the cell center or along the cell margin at a rate of 0.29±0.24 μm minute^{-1}. Photobleaching and recovery experiments with evanescent illumination revealed that the integrins at the extending tip of the clusters were supplied from the intracellular space. Simultaneous time-lapse imaging of exocytosis of integrin-containing vesicles and elongating focal contacts showed that most exocytosis occurred at or near the focal contacts followed by their elongation. Double staining of F-actins and integrins demonstrated that stress fibers were located near the integrin clusters and that intracellular punctate integrins were associated with these stress fibers. These results suggest that the clustering of integrins is mediated by actin-fiber-dependent translocation of integrins to the extending tip of focal contacts.

Key words: Focal contact, Evanescent light microscopy, Integrin, Cytoskeleton, Endothelial cells

INTRODUCTION

Vascular endothelial cells in vivo show a spindle-like shape aligning with their long axis, which runs along the vessel. Focal contacts (FCs) via integrins play a crucial role in maintaining the shape of the endothelial cells (Drake et al., 1992), as in many other cell types (Kumar, 1998). Integrin is a heterodimeric complex composed of noncovalently associated α and β chains. In mammals, 17 subtypes of the α subunit and eight subtypes of the β subunit are known. These α and β subunits heterodimerize to produce 22 different receptors (Kumar, 1998). Endothelial cells express a number integrin subtypes, two of which ($\alpha_5\beta_1$ and $\alpha_v\beta_3$) are known to be important for FC formation (Luscinskas and Lawler, 1994; Ruoslahti and Engvall, 1997). In particular, $\alpha_5\beta_1$, which binds an Arg-Gly-Asp (RGD) tripeptide in fibronectin (Ruoslahti, 1996), is important for vascular development and maintenance of vascular integrity.

Two types of cellular mechanism have been proposed for integrin clustering. The first model suggests that the clustering is dependent on the lateral diffusion of integrins in the plasma membrane (Sheets et al., 1995; Miyamoto et al., 1995; Regen and Horwitz, 1992). It is conceivable that unoccupied integrins that have been released from the substrate at the rear of the cell diffuse laterally in the plasma membrane and arrive at the leading edge to become a source for making fresh FCs. However, it is unclear in this scheme why they would not attach to the substrate again before reaching the leading edge, where they are needed. The second model suggests that intracellular integrins, which have already been internalized from the cell membrane, are translocated to the site where FCs are newly formed (Lawson and Maxfield, 1995; Bretscher, 1989). Exocytosis of vesicles carrying integrins was suggested to be a mechanism to supply integrins for newly forming FCs at the leading edge of migrating cells (Stossel, 1993; Lawson and Maxfield, 1995). It is known that circulating proteins such as transferrin, low density lipoprotein and ferritin receptors are returned to the cell surface at the leading edge of spreading or moving cells (Bretscher, 1983; Bretscher and Thomson, 1983; Ekblom et al., 1983). However, many of these studies used morphological observations of fixed samples and/or biochemical evaluations. Recently, there have been several studies of the morphological changes of FCs (Regen and Horwitz, 1992; Smilenov et al., 1999; Zamir et al., 2000; Pankov et al., 2000). These observed the movement of the cell surface integrins in migrating fibroblasts and demonstrated the relationship between the movement of FCs and stress fibers. However, the precise cellular mechanisms of integrin clustering are not clearly understood during the formation of the FCs in living human umbilical vein endothelial cells (HUVECs).

High-resolution imaging of the clustering process of integrins in living cells is crucial to understanding the molecular mechanism of integrin clustering during FC formation. Total-internal-reflection fluorescence (TIRF) microscopy is potentially useful to visualize the cell-substrate contact region (Schwartz et al., 1980; Tatsumi et al., 1999). Because this contact region is selectively illuminated by evanescent light in TIRF microscopy, fluorescence from fluorophores both in the bulk solution and inside the cells are significantly suppressed compared with epifluorescence (EpiF) microscopy. Using this TIRF imaging system, we have analyzed the process of integrin clustering during FC formation in HUVECs.

MATERIAL AND METHODS

Cell preparation

Endothelial cells were prepared from a human umbilical cord vein as described previously (Grimbrone, 1976). In brief, a human umbilical cord was aseptically removed from the placenta immediately after a birth. The vein was washed with phosphate-buffered saline (137 mM NaCl, 8.10 mM Na_2HPO_4, 2.68 mM KCl, 1.47 mM KH_2PO_4, pH 7.40), followed by treatment with 0.2% trypsin for 10 minutes. The perfusate was centrifuged at 1,500 rpm for 10 minutes and the resulting cells were washed with phosphate-buffered saline, plated in 35 mm plastic dishes and maintained in Humedia-EG2 (Kurabo, Osaka, Japan), which was made by modifying the MCDB 131 medium. Cells used in this study were within two to three passages.

Fluorescent staining of integrins in living HUVECs

HUVECs removed from a culture dish were transferred onto a handmade chamber for TIRF microscopy (described below) and were incubated with FITC-labeled monoclonal antibodies against the extracellular domain of integrin β_1 subunit (FITC-anti-β_1-integrin; CD29, ENDOGEN, USA) for 30-90 minutes (1:50 dilution). After washing the dye three times, the chamber was moved onto a stage of a multimode imaging microscope (described below). In some experiments, HUVECs were incubated without the above antibody for 2 hours and were fixed with 2% paraformaldehyde. The specimen was labeled with the same monoclonal antibody against the extracellular domain as above or with that against the intracellular domains of the β_1 subunit (CD29, DAKO, Denmark). The latter antibody was further labeled with secondary rhodamine-labeled antibody. The staining patterns of FCs labeled with the antibodies were exactly the same with or without preincubation with the antibody against the extracellular domain of the β_1 subunit. This result demonstrated that the antibody used for the live imaging did not perturb the integrin clustering and that integrin dynamics can be imaged by an FITC-labeled antibody against extracellular domains of the β_1 subunit in living cells.

For the simultaneous live imaging of exocytosis and integrin clustering, cells were treated with both anti-β_1-integrin antibody and FM4-64 (1 μM, Molecular Probes, USA), a fluorescent styryl dye, that can selectively label transport vesicles (Henkel and Betz, 1995). The simultaneous observation was made 1 hour after plating the cells.

To examine co-localization of β_1 integrin with vinculin, FITC anti-β_1-integrin antibody-labeled HUVECs were cultured for 2 hours and fixed with 2% paraformaldehyde, permeabilized by 0.5% Triton X-100 and blocked with unlabeled goat anti-mouse IgG (Chemicon International) to suppress the nonspecific staining. This sample was incubated with anti-vinculin (mouse monoclonal, clone V284, Upstate Biotechnology) and TRITC anti-mouse IgG (DAKO, Denmark). No TRITC staining was seen without anti-vinculin treatment.

Multimode microscopy

TIRF optics were incorporated into an inverted microscope (Axiovert 135M; Zeiss, Germany) with differential interference contrast (DIC), EpiF illumination, confocal laser-scanning fluorescence (CLSF) and reflection interference contrast (RIC) optics. Video-enhanced DIC imaging was used to examine the details of the cell structures and EpiF imaging to monitor the intracellular distribution of FITC-antibody-labeled integrins and transport vesicles. A CLSF microscope (Radiance 2000; Bio-Rad, USA) was used to analyze the three-dimensional distribution of the integrins, particularly those near the submembrane region (1 μm above the substrate). For RIC imaging, the EpiF mirror was simply replaced with a 50% mirror and each specimen was illuminated with red filtered (610 nm) light. RIC microscopy was used to view FCs to clarify whether the TIRF images of integrins originated from FCs.

The chamber for the multimode imaging microscope consisted of a 0.25-0.35 mm soda-lime-glass cover slip (No. 3, Matsunami, Japan) and a rectangular prism. The laser beam (473 nm, 3-18 mW, attenuated to 10 mW (Solid State 473, HK5510, Shimadzu, Japan) or 532 nm, 5 mW, (DPSS532, Coherent, USA)) was directed into the rectangular prism (2 mm height BK-7 glass prism, refractive index= 1.522, Nihon Ryokyo, Japan). The incident beam propagates in the glass cover slip towards the optical axis of the microscope via multiple internal reflections. The diameter of the each spot of laser light at each internal reflection was ~500 μm. The incident angle (θ) in our experimental condition was 70°. The depth (D_p) of the evanescent light penetration (surface light intensity divided by e) was estimated to be 75 nm for 473 nm light using Eqn 1 (Burmeister et al., 1994; Zhu et al., 1986):

$$D_p = \lambda \div (4\pi n_1) \sqrt{(\sin^2\theta - (n_2/n_1)^2)} \quad (1)$$

where λ is the wavelength of the laser light, n_1 and n_2 are the refractive indices of glass and water, respectively. Because the actual penetration depth depends on the refractive index of the medium and the flatness of the substratum, the penetration depth of evanescent light was experimentally examined in a previous study (Tatsumi et al., 1999). TIRF microscope images were focused on a cooled-CCD camera (Micromax, Princeton Instruments, USA) after passing through a 510 nm or 560 nm long-wave-path filter (for green fluorescence from labeled integrins), or a 590 nm long-wave-path filter (for red fluorescence from labeled actins or transport vesicles). The images obtained were processed with the programs MetaMorph (Universal Imaging, USA) and Photoshop (Adobe). During the experiment, the temperature of the chamber was maintained at ~37°C.

In the bleaching and recovery experiments, a higher power of laser (18 mW, 30 seconds exposure) was used to bleach the FITC fluorescence only in the evanescent field, and the recovery of the fluorescence was examined with smaller power and short exposure of the laser light (1 mW, 1 second).

Drugs

The drugs used were cytochalasin D (Sigma), butanedione monoxime (BDM; Sigma), ML9 (Biomol, USA), ML7 (Biomol, USA), colchicine (Sigma); bodipy-labeled phalloidin (Molecular Probes, USA), antibodies for integrin (FITC-anti-β_1 integrin; anti-human CD29, ENDOGEN, USA or anti-human CD29, DAKO, Denmark), octadecyl rhodamine-B chloride (O246, Molecular Probes, USA), FM4-64 (Molecular Probes, USA), goat anti-mouse IgG (Chemicon International, USA), anti-vinculin (mouse monoclonal, clone V284, Upstate Biotechnology, USA) and TRITC-anti-mouse IgG (DAKO, Denmark). Other drugs were from Sigma (USA) or Wako (Japan).

RESULTS

Process of FC formation in HUVECs

HUVECs stained with antibody against the integrin β_1 subunit were incubated under the standard culture conditions and were

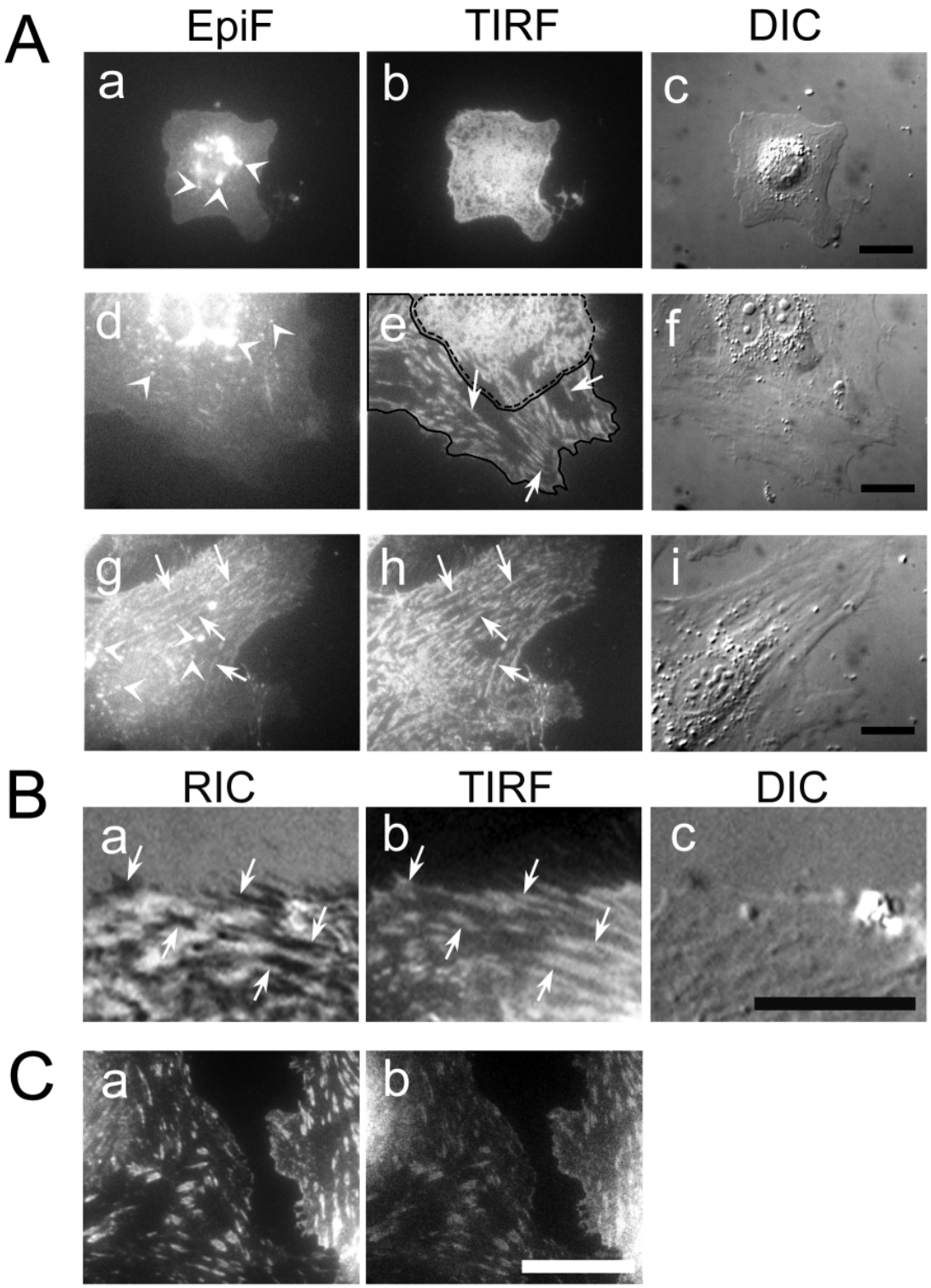

Fig. 1. Integrin clustering during FC formation. (A) HUVECs were fixed at 30 minutes (a-c), 1 hour (d-f) and 6 hours (g-i) after plating. The left-hand column shows EpiF images, the middle column TIRF images and the right-hand column DIC images of the cells at different time after plating; images in each line are from the same cell. At 30 minutes after plating (a-c), a uniform distribution of integrins is observed in >90% of the bottom area of the cell (b). At 1 hour (d-f), a dappled distribution of integrins (the region surrounded by a broken line in e) and clusters of integrin are seen. Arrows show typical clusters of integrins in the region surrounded by a continuous line in e. At 6 hours after plating (g-i), clusters of integrins cover the entire bottom surface of the cell (four typical examples are indicated by arrows in h); arrows in g and h show the same integrin clusters. Integrins in the bottom surface of the cell were imaged more clearly by TIRF microscopy than by EpiF microscopy. Arrowheads in a, d and g show the punctate spots of integrins near the cell nucleus. (B) Integrin clusters observed by TIRF (arrows in b) correspond to the dark areas in the RIC image (arrows in a) of a HUVEC at 2 hours after plating. (C) Integrin clusters observed by EpiF (a) correspond to the vinculin clusters in the EpiF image (b) of the same HUVECs at 2 hours after plating. Bars, 20 μm.

fixed at various times (30 minutes to 6 hours after plating) to examine the clustering process of integrins using multimode imaging microscopy. Integrins were uniformly distributed over the basal surface of the cells at 30 minutes after plating (Fig. 1Ab). At 1 hour after plating, a dappled pattern of integrins (Fig. 1Ae, region surrounded by a broken line) and scattered clusters of integrins (Fig. 1Ae, indicated by arrows in the region surrounded by a continuous line) became visible. At 6 hours, clusters occupied the entire basal surface of the cells (Fig. 1Ah, arrows). The clusters could be observed by either EpiF or TIRF microscopy (Fig. 1Ag,h, arrows). However, the images observed by TIRF microscopy were much clearer because of the lower background fluorescence noise. Most of the clusters observed by TIRF microscopy (Fig. 1Bb, arrows) almost matched the dark-contrast contact regions in RIC images (Fig. 1Ba, arrows). The distribution and shape of the integrin clusters were in good agreement with those of the vinculin clusters in the EpiF images of HUVECs at 2 hours after plating (Fig. 1C). These results strongly suggest that the clusters of integrins observed with the TIRF microscope were FCs. The morphology of the cell membrane was examined by staining the cell membrane with O246, an octadecyl rhodamine-B chloride (Tatsumi et al., 1999), and the result showed that the membrane was almost flat, being located immediately above the cover slip with a small clearance (data not shown). These results confirmed that integrin clusters at FCs were selectively imaged in the living cell membrane by TIRF microscopy. Analysis of TIRF images showed that the average width of integrin clusters at FCs was 1.06±0.31 μm (n=50), and their average length was 7.02±1.34 μm (n=50) at 6 hours after plating. A similar observation was reported in fibroblasts (LaFlamme et al., 1992).

The distribution of integrins in the whole cell body was examined by EpiF microscopy. At 30 minutes (or sometimes 1 hour) after plating, punctate spots of integrins were observed around the nucleus (Fig. 1Aa,d, arrowheads), which were not seen in TIRF images (Fig. 1Ab,e), indicating that they were located in the intracellular space. At 6 hours after plating, the punctate spots of integrins around the nucleus decreased and those at FCs increased (Fig. 1Ag). These results suggest that the surface integrins labeled with the FITC antibody were internalized, accumulated around the nucleus and translocated to the ventral surface of the cell being recruited to the FC formation.

Time-lapse imaging of integrin cluster formation at FCs

The dynamic process of the formation of integrin clusters at

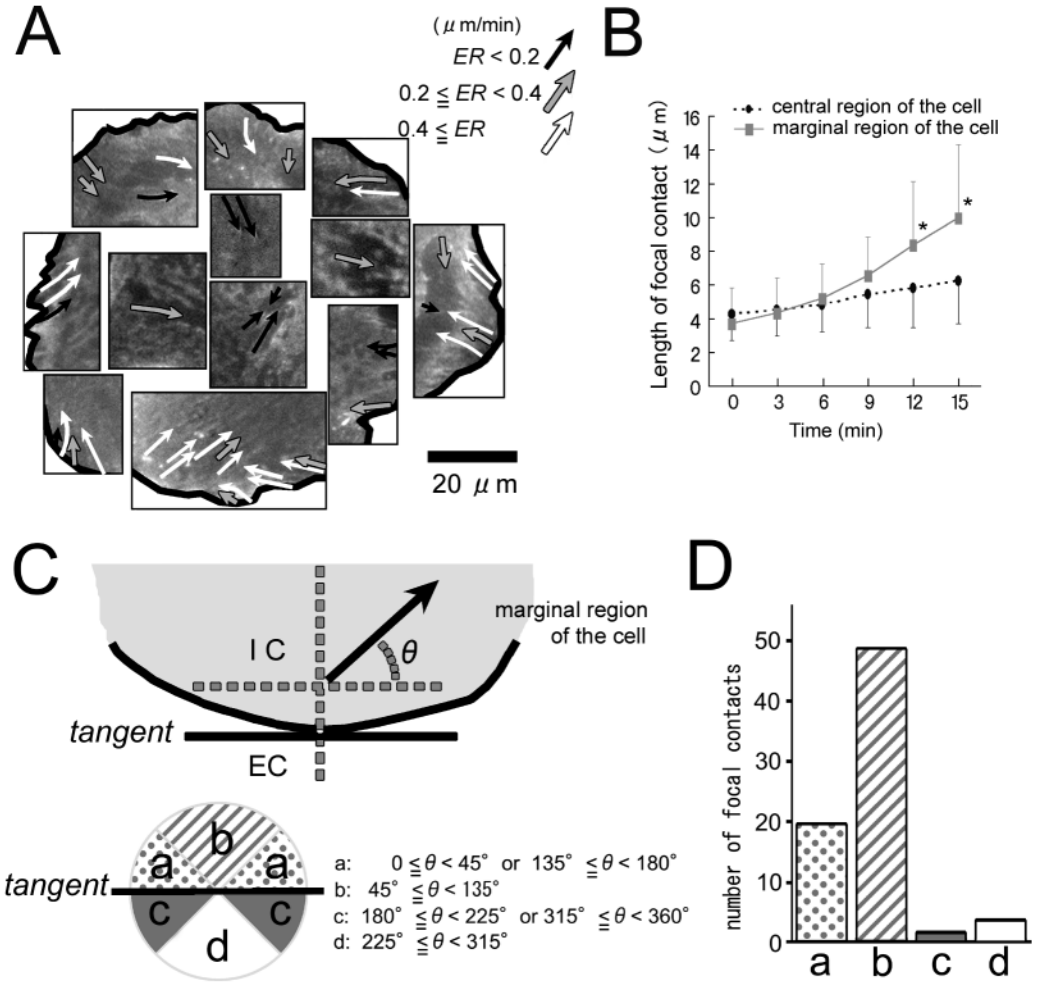

Fig. 2. Analysis of the elongation of integrin clusters at FCs. (A) A composite TIRF image of 12 cells with superimposed arrows that indicates the direction of elongation of the integrin clusters. Each TIRF image was taken from a region of the cell where active elongation of integrin clusters at FCs was seen. Each arrow shows the gross shape and length of a cluster analyzed and the direction of its elongation. The brightness of the arrow indicates the elongation rate (ER) of the cluster. For example, white arrows show the FCs that elongated with a rate greater than 0.4 μm minute^{-1} and black arrows a slower elongation rate (<0.2 μm minute^{-1}). (B) Time courses of elongation of integrin clusters at FCs located at the marginal and central regions of the cells. The elongation rate at the marginal region was significantly higher than that in the central region at 12 minutes and 15 minutes. (C) The relative direction (θ) of the elongation was measured with respect to the horizontal axis that approximates a tangent to the cell margin nearest to the cluster. (D) Histogram of the direction distribution of the elongation. Each bar indicates the numbers of elongating clusters with different directions (θ) defined in (C).

FCs was examined in living cells by time-lapse TIRF microscopy. TIRF images were recorded every 3 minutes from 1 hour after plating for 15 minutes, because cells showed most active integrin clustering at FCs between 1 hour and 2 hours after plating. Analysis of the integrin clustering at FCs (329 FCs from 10 cells) during the first 30 minutes showed that 10% of FCs were elongated, 3% were shortened and 87% were unchanged. The average length of the unchanged FCs at 2 hours after plating was 7.01±1.64 μm (n=50). This value was similar to that of FCs at 6 hours after plating, suggesting that the FCs with this length were matured. There were no differences in the size and density of the FCs between the cells that were incubated with the antibody against extracellular integrin and the cells without incubation with the antibody (see Methods). The period necessary for FC formation (2 hours) was the same in control HUVECs and anti-integrin-antibody-treated HUVECs. These observations suggest that the anti-β_1-integrin antibody was non-perturbing.

Unidirectional elongation of integrin clusters was usually observed over the entire ventral surface of the cells (Fig. 2). The elongation rate and direction of individual integrin clusters were calculated from time-lapse images. The values obtained are summarized in Fig. 2A, demonstrating a clear tendency for the elongation rate in the central region of the cell to be lower than that in the marginal region of the cell. The elongation rate of integrin clusters within 10 μm of the cell margin was 0.42±0.29 μm minute^{-1} (n=15) and that in the central region was 0.17±0.06 μm minute^{-1} (n=15), which is significantly lower (P<0.01) (Fig. 2B).

The directions of the elongation of integrin clusters were examined in 72 cases. Most of the integrin clusters at FCs elongated towards the center of the cell (68%, Fig. 2Db), and very few integrin clusters were towards the cell margin (4%, Fig. 2Dd). The remainder had intermediate orientations (Fig. 2Da,c).

The intensity profile of the fluorescence of individual elongating integrin clusters at FCs were measured to clarify the details of the FC elongation (Fig. 3). The fluorescence intensity at the extending tip of the integrin clusters in the central region of the cell was relatively low compared with that of the middle part of the integrin cluster and became higher during elongation (Fig. 3A). However, the intensity of fluorescence at the extending tip of the integrin clusters at the marginal region of the cell was always high during elongation (Fig. 3B, arrowheads). These results suggest that a relatively small amount of integrin was supplied at the extending tip of FCs in the central region, whereas a large amount of integrin was supplied at the tip of FCs at the marginal region of the cell.

Transport and turnover of integrins

Photobleaching and recovery of fluorescence have been used in various studies to determine the movement of fluorescently labeled molecules (Mallavarapu and Mitchison, 1999; Nakata et al., 1998; Oancea et al., 1998). Photobleaching by

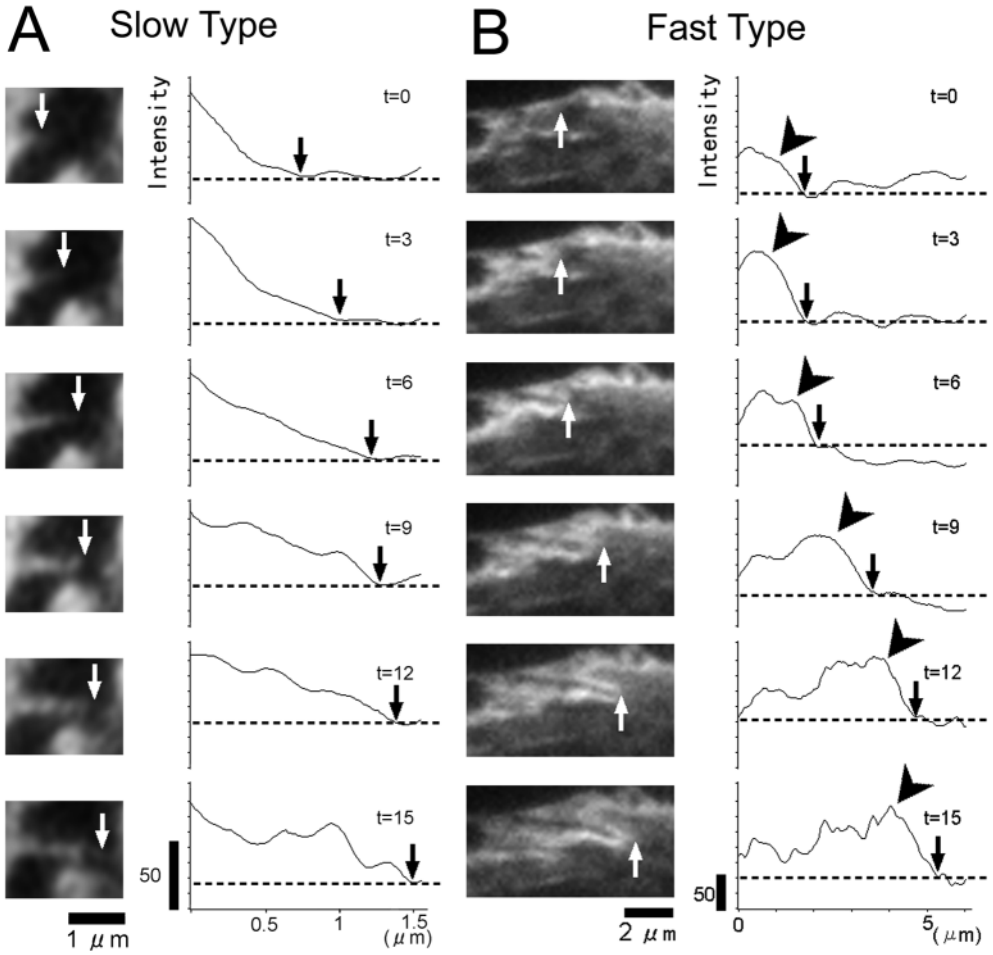

Fig. 3. Time-lapse TIRF images of the elongation of individual integrin clusters at FCs. (A) Time-lapse TIRF images of integrin clustering for 15 minutes of recording. The left-hand column shows a series of TIRF images of an elongating integrin cluster in the central region of the cell. The right-hand column shows the corresponding fluorescence intensity profiles (arbitrary unit; a.u.) along the elongation path. Arrows show the tip of the integrin cluster, extending to the right. (B) A series of TIRF images of an elongating integrin cluster at the FC near the marginal region of the cell. Arrows point to the tip of an integrin cluster. The right-hand column indicates the corresponding fluorescence intensity profiles of the integrin cluster, showing that the extending cluster is brighter near the tip (arrowheads) and grows faster than those at the central region of the cell.

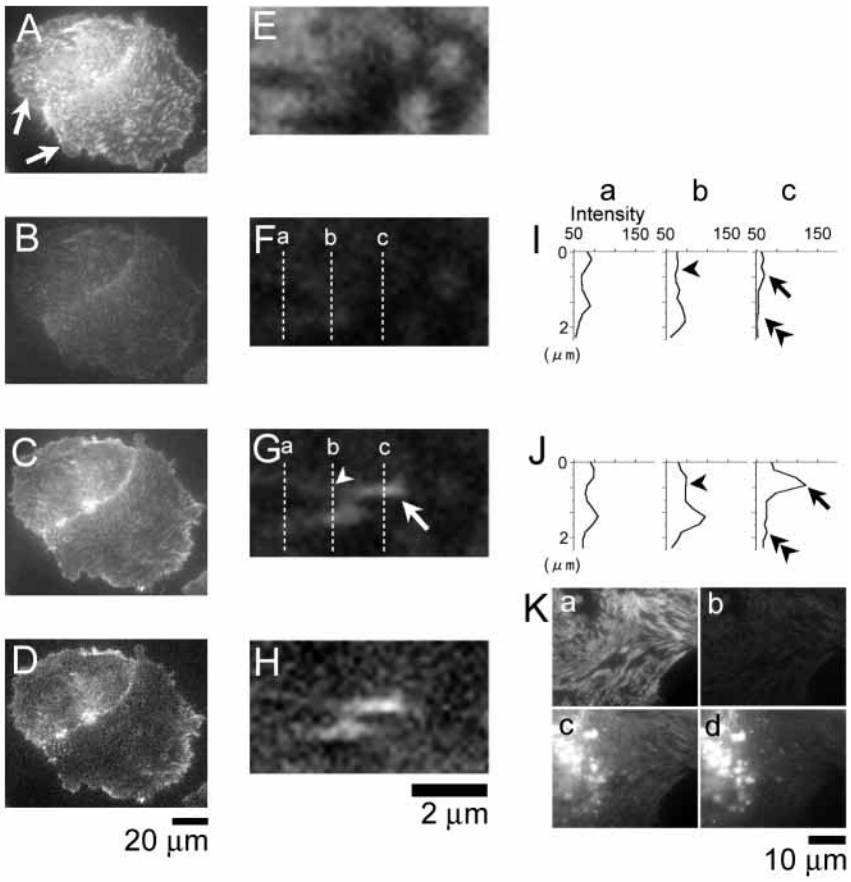

Fig. 4. Photobleaching and recovery of the fluorescence. The two columns show a photobleaching and recovery process in two cells (A-D) and that of two integrin clusters at FCs (E-H), respectively. A and E show control TIRF images; B and F are those just after photobleaching; C and G are those after 15 minutes of recovery. D and H show the result of subtracting B from C and F from G, respectively. Two arrows in A point out the two cells, separated by a bright border. The arrow in G shows the intensive recovery of integrin fluorescence at the extending tip of the integrin cluster, and the arrowhead in G demonstrates the relatively weak recovery of fluorescence in the preformed cluster. I and J show the fluorescence intensity profile along the broken lines (a-c) shown in F and G. The three profiles in I were measured immediately after photobleaching and those in J after 15 minutes of recovery. Arrows in I and J show the intensity at the extending tip of the integrin cluster recovered in G, arrowheads in I and J show a preformed part of the integrin cluster, and double arrowheads show the background level of fluorescence near the tip. Upon photobleaching, the fluorescence decreased to ~60 counts from the original 150 counts. A strong recovery was then seen at the tip of the integrin cluster (Jc, arrow), whereas the recovery was relatively small at the middle of the integrin cluster (Jb, arrowhead) and in the background (Jc, double arrowhead). (K) Control images (a,c) and images immediately after photobleaching (b,d); all images are from the same cell. The TIRF image (b) shows that the FITC anti-β_1-integrin antibody fluorescence at the ventral surface of the cell was faded after photobleaching. The EpiF image (d) shows that the intracellular FITC fluorescence remains intact after photobleaching.

evanescent light allows photobleaching of FITCs conjugated with integrins only at the ventral surface of the cell, while keeping the intracellular FITCs (conjugated with integrins) intact (Fig. 4K). FITC-stained HUVECs were illuminated by an intense 473 nm laser beam (18 mW, 30 seconds) for photobleaching. The mean intensity of the TIRF of single cells immediately after the onset of photobleaching illumination was 45% of the control and it returned to the control level at 15 minutes or more after the illumination. Strong recovery of fluorescence was seen near the cell margin and the boundary between the two cells, whereas the recovery was relatively weak in the central region of the cell (Fig. 4, left column). If the florescence recovery was caused by lateral diffusion of unbleached labeled integrins in the apical cell surface, there should be a time-dependent gradient of recovery from the marginal to central region of the basal area. However, such a phenomenon was not observed. These findings demonstrate that integrins were supplied to the ventral surface of the cell from the intracellular region, and that the amount of integrins supplied around the cell margin and the junctional area between the cells was larger than that in the central region of the cell. This larger supply of integrins at the cell marginal region might be one of the causes of the larger rate of elongation of the integrins at the marginal regions of the cell in Fig. 3.

Photobleaching and recovery of 68 integrin clusters at FCs in the high magnification images were analyzed to examine the amount of integrin supplied to individual FCs. The fluorescence intensity of integrins was determined at the extending tip of the integrin clusters (85% of observations (n=68; Fig. 4G)) or diffusely along the preformed integrin clusters (15% of observations). Quantitative representation of a typical recovery of fluorescence after photobleaching is shown in Fig. 4E-J, demonstrating that the fluorescence at the extending tip of the integrin cluster increased from 61 to 133 counts (Fig. 4, arrows in I and J). However, fluorescence at the middle part of the integrin cluster, which existed before photobleaching, increased from 66 to 83 counts (Fig. 4, arrowheads in I and J). Fluorescence also recovered slightly at the outside of the integrin clusters (Fig. 4, double arrowheads in I and J). Subtraction of a photobleached image from a recovered one shows more clearly the intensive recovery at the extending tips of the integrin clusters at FCs (Fig. 4H). These findings suggest that the intracellularly distributed integrins were translocated mainly to the tip of elongating FCs. Relatively weak recovery of fluorescence in the pre-existing clusters suggested that integrins in the cluster maintained their turnover with a lower supply rate than that at the extending tip. Weak recovery of fluorescence outside FCs suggested that integrins were also translocated to the cell membrane but that the amount of integrin supplied was lower than that of FCs.

Source and mechanism of integrin supply to the FC formation

The distribution of integrins slightly above the integrin cluster at FCs was imaged by CLSF microscopy to examine the source of integrin supplied to the extending tip of FCs. Time-lapse recordings of integrin clusters at FCs were carried out by interchangeable TIRF and CLSF microscopy at 1 hour after plating (Fig. 5). CLSF images at 1 μm above the basal surface of the cell showed the punctate spots of integrins remained near the extending tip of the integrin clusters at FCs in 32% (n=110) of the cases observed. In the remaining cases, diffuse fluorescence images of integrins were observed near the integrin clusters at FCs. These findings suggested that intracellular integrins near the tip of FCs could be a source of integrins that can be used for the FC formation.

One of the most likely mechanisms for the supply of integrins to FCs is that it is mediated by an exocytosis of the vesicles that contained the integrins. To examine the involvement of exocytosis in the FC formation, cells were treated for 30 minutes with FM4-64 and then washed. The exocytosis process during the formation of integrin clusters was imaged using FM4-64. When cells were stained with FM4-64 and anti-β_1-integrin antibody, most of the intracellular vesicles (60%, n=158) were positive for both FM4-64 and integrins, suggesting that integrins were carried by vesicles (Fig. 6Aa,b). The number of FM4-64 fluorescence spots declined gradually, probably because of the exocytosis of FM4-64 (Fig. 6Ac). To examine the relationship between exocytosis of FM4-64 and FC formation at the basal region of the cells, we made simultaneous TIRF images of vesicles and integrins. Fig. 6Ba,b show the images of two vesicles (indicated by arrows in a) and integrins located at the corresponding positions of the vesicles (indicated by arrows in b), just above an elongating FC. It is very likely that these vesicles contain integrins from the fluorescence images. Fig. 6Bc,d show the images taken 3 minutes after images a and b, and that the FM4-64 florescence of two vesicles had disappeared from their original positions (Fig. 6Bc), while

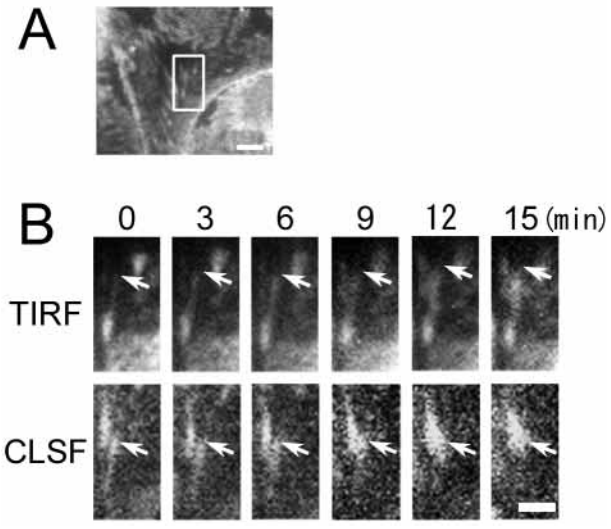

Fig. 5. Simultaneous time-lapse imaging of integrin clusters at FCs by TIRF and CLSF microscopy. (A) A TIRF image of integrin clusters at 90 minutes after plating. The area surrounded by a rectangle was magnified and their dynamics were imaged by time-lapse TIRF and CLSF microscopy for 15 minutes as shown in B. Elongation of an integrin cluster at an FC was observed in the upper series of TIRF images (an arrow in each frame shows the tip of an extending integrin cluster), and a punctate spot of integrins in the intracellular space (an arrow in the lower series) was located slightly (~1 μm) above the tip of the integrin cluster at the FC. Bars, 10 μm (A) and 5 μm (B).

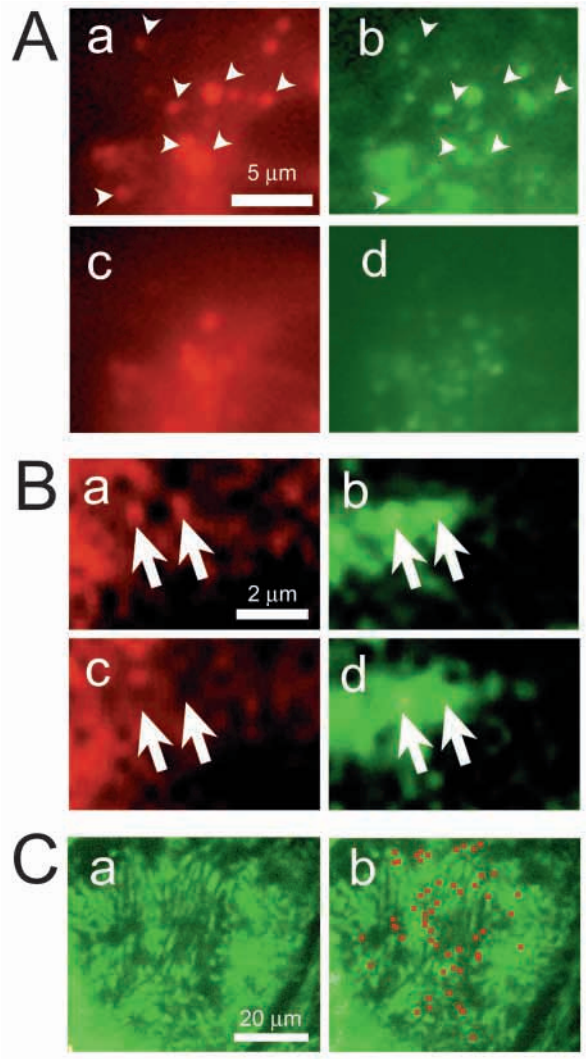

Fig. 6. Time-lapse imaging of exocytosis and elongation of FCs. HUVECs were double stained with FM4-64, a marker for transport vesicles, and fluorescent anti-β_1-integrin antibody for 30 minutes before plating. (A) EpiF images observed at 60 minutes (a,b) and 90 minutes (c,d) after plating; (a,c) fluorescence spots from vesicles; (b,d) fluorescence spots from integrins. Arrowheads in a and b indicate the spots positive for both vesicles and integrins. The number of fluorescence spots decreased gradually, suggesting the progress of exocytosis (c). (B) TIRF images were observed 60 minutes (a,b) and 63 minutes (c,d) after plating. (a,c) The disappearance of fluorescence spots from vesicles (arrows). (b,d) The fluorescent spot from integrins and the spread of the bright integrin cluster. (C) TIRF images of the elongation of FCs. Images were taken at 60 minutes (a) and 75 minutes after plating (b). Red dots in b show the location of vesicle disappearance (putative exocytosis) during 15 minutes of observation.

the fluorescence of the integrins spread along the FCs, suggesting an elongation and spread of the FC (Fig. 6Bd). The sudden disappearance of FM4-64 fluorescence from the vesicles within a relatively short period and the stable or increased intensity and size of the fluorescence from the integrins that were suggested to be in those vesicles strongly suggested the exocytosis of FM4-64 and the incorporation of integrins into FCs. Simultaneous time-lapse TIRF imaging using FM4-64 and anti-integrin antibody for a longer period (15 minutes) showed that 45% of the FM4-64 fluorescence spots disappeared at or near the extending tip of FCs (less than 1 μm from the tip) (Fig. 6C); 25% of the fluorescence spots disappeared in the central part of FCs and the remaining fluorescence spots (30%) disappeared outside the FCs. These observations, together with those from photobleaching and the recovery experiments, suggested that the exocytosis of integrin-containing vesicles is the major mechanism by which integrins are supplied to the FCs in the basal membrane. FM4-64 can be used as a marker for endocytosis of vesicles in general, but in the present experimental condition, endocytosis of FM4-64 was not seen, because the diffusion of the dye was too rapid to label the membrane after exocytosis.

Colocalization of integrins with stress fibers

Association of F-actins with FCs has been reported in various types of cell (Kumar, 1998). Spatial distributions of stress fibers and integrins in intracellular space and near the integrin clusters at FCs was examined by CLSF and TIRF microscopy at various times during FC formation. Cells were fixed at 30 minutes, 1 hour and 6 hours after plating, and were double-stained for F-actins and β_1 integrins. Sectioning images were taken at 1 μm above the basal plane of the cell by CLSF microscopy. At 30 minutes after the cell plating, the labeled integrins were colocalized with F-actins, particularly at the marginal region of the cells (Fig. 7Ac, arrows). At 1 hour after plating, 95% of the fluorescence spots of β_1 integrins were localized along the stress fibers (Fig. 7Ad,e,f; arrows and arrowheads). Essentially the same result was obtained at 6 hours after plating (Fig. 7Ai). The spatial distributions of stress fibers and integrins at the cell bottom were imaged simultaneously by TIRF microscopy (Fig. 7B). Stress fibers were located along the bottom of the cell and they often terminated at integrin clusters at FCs (Fig. 7B, arrows). The CLSF images of integrins and stress fibers showed the co-localization of integrins and stress fibers in the intracellular space. Most of the integrins were located along the intracellular

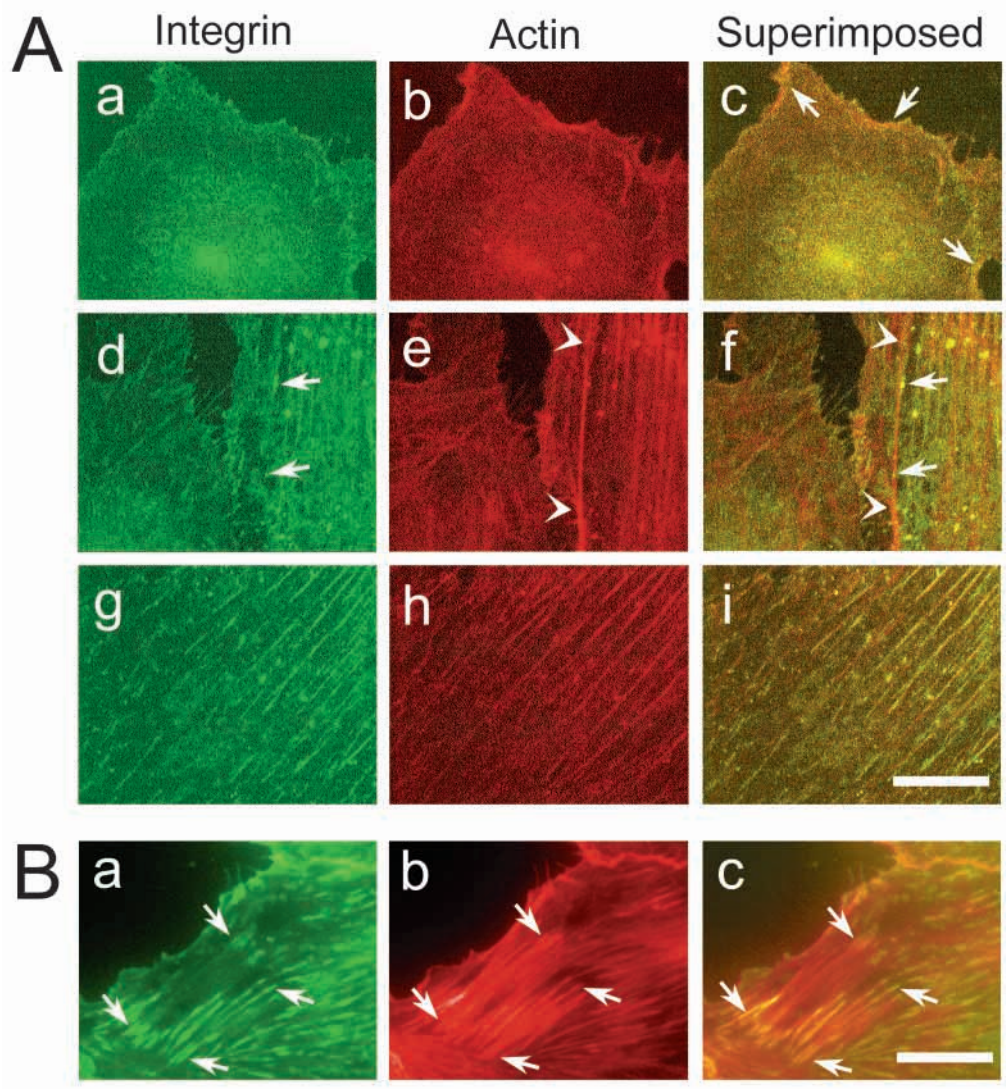

Fig. 7. Colocalization of integrins and stress fibers imaged by CLSF and TIRF microscopy. (A) HUVECs were fixed 30 minutes (a-c), 1 hour (d-f) and 6 hours (g-i) after plating. The left-hand column shows the images of integrin distribution (a,d,g); the centre column shows stress fiber distribution (b,e,h); the right-hand column shows superimposed images of the corresponding images in the left and centre columns (c,f,i). These images were taken 1 μm above the basal plane of the cell with a CLSF microscope. At 30 minutes after plating, integrins were colocalized with F-actin at the marginal region of the cell (arrows in c). Arrowheads in e and f indicate a typical stress fiber. At 1 hour after plating, the integrin clusters were located along the stress fibers (two arrows in d and f show typical cases). The same trend was observed in integrin cultures at 6 hours after plating (g-i). (B) HUVECs were fixed at 1 hour after plating and observed by TIRF microscopy. (a) A TIRF image of integrin clusters at FCs; (b) stress fibers; (c) superimposed images of a and b. Bright images of integrin clusters can be seen at the ends of stress fibers (arrows in a-c). Bar, 20 μm.

stress fibers at 2 hours after plating. This supports the idea that most of the integrins are translocated along the intracellular stress fibers. These findings also agree with those from the photobleaching experiment, because these intracellular integrins (FITC) were not bleached by evanescent light illumination.

Inhibition of integrin clustering at FCs by cytochalasin D, BDM and ML9

Both actin-based and microtubule-based intracellular translocation systems have been reported previously (Hirokawa, 1998; Mermall et al., 1998). The effects of drugs that block these translocation mechanisms on the formation of integrin clusters at FCs were examined. At 1 hour after plating, the cells were treated with cytochalasin D (30 nM), BDM (10 mM; an inhibitor of non-muscle myosin II and myosin V adenosine triphosphatases (Cramer and Mitchison, 1995)), ML9 (10 μM) or ML7 (10 μM) (blockers of myosin-light-chain kinase (Saitoh et al., 1987)) for 1 hour and examined for FC formation by TIRF or EpiF microscopy. In the presence of cytochalasin D and BDM, 90% of integrin clusters at the FCs disappeared and the remaining integrin clusters at FCs were thinner and shorter than the controls. Punctuate spots of integrins were observed around the nucleus. Similar inhibitory effects were seen in ML9-treated specimens. However, ML7 showed less inhibitory action than ML9 as shown by a biochemical study (Saitoh et al., 1987). Colchicine had no effect on the formation of integrin clusters at FCs. All of these findings suggest the importance in FC formation of actomyosin-dependent translocation of integrins.

DISCUSSION

Translocation of integrin clusters and the formation of FCs have mainly been studied in fibroblasts (Bretscher, 1989; Smilenov et al., 1999; Zamir et al., 2000). These studies demonstrated the translocation of integrins in migrating cells from the trailing edge (tail) to the extending margin (head) of the cell, where new adhesive contacts are formed. A possible process of integrin translocation can be summarized as follows: (1) endocytosis of integrins at the leaving edge (Bretscher, 1989; Altankov and Grinnell, 1995; Palecek et al., 1996); (2) translocation of vesicles containing integrins to the perinuclear region (Bretscher, 1989; Sczekan and Juliano, 1990; Tawil et al., 1993; Altankov and Grinnell, 1995); and (3) further translocation of integrins to newly constructing FCs (Lawson and Maxfield, 1995). The punctate spots of integrins near the cell nucleus observed at 30 minutes after cell plating in the present study agrees with the above hypothesis that the integrins were taken up into the cell by endocytosis from the cell surface and translocated to the perinuclear region. The dappled image of integrins at 1 hour after plating might also be due to the endocytosis of integrins at the basal cell membrane. Because these punctate spots disappeared after the formation of integrin clusters at FCs, the integrins at the perinuclear region would be translocated to the basal cell membrane to construct new FCs. We mainly examined this process in this study.

Two hypotheses for the construction of new FCs have been proposed. First, lateral diffusion of integrins in a local region of the cell membrane (Sheets et al., 1995), which was suggested to be necessary for FC formation (Miyamoto et al., 1995). Second, vesicles that contain integrins translocate from the intracellular space to FC-forming sites (Lawson and Maxfield, 1995). The present findings support the latter hypothesis, because the photobleaching and recovery experiments by evanescent illumination strongly suggested that integrins were supplied from the intracellular space to the elongating site of FCs. Analysis of the intensity profile of integrin fluorescence and simultaneous imaging of elongating FCs by CLSF and TIRF microscopy also support the latter hypothesis. Furthermore, the EpiF (or CLSF) imaging of integrins demonstrated that most were condensed near the nucleus after the endocytosis of the integrins at 30 minutes after the plating and, at 6 hours, these punctate spots of integrins around the nucleus decreased (or disappeared) while those at FCs increased, suggesting that most of the integrins were supplied from intracellular space. Simultaneous imaging of exocytosis of integrin-containing vesicles and elongation of FCs also suggested that the supply of integrins to FCs was mediated by exocytosis. Fig. 8 summarizes our hypothesis for integrin translocation and FC formation. The extension of integrins towards the cell centre might be due to a direct incorporation of integrins by exocytosis to the tip of FCs and/or the lateral translocation of integrins that originated from exocytosis near the tip of FCs. However, we do not exclude the possibility that part of the integrins incorporated in the tip of the elongating FCs could arise from the bleached cell-surface integrins that could not be seen after photobleaching. It is plausible that surface integrins will turn over for a long time. The integrins supplied at the tip of FCs could also be recycled slowly because the site of adhesion could turn over.

In this study, we could recognize certain spots of integrins and their colocalization with short filaments of actins at the marginal region of the cell at 30 minutes after cell plating, where no stress fibers and no punctate spot of integrins were seen. This suggests that integrins aggregate by lateral diffusion and form a premature adhesive contact during an early stage of FC formation at the marginal region of the cell.

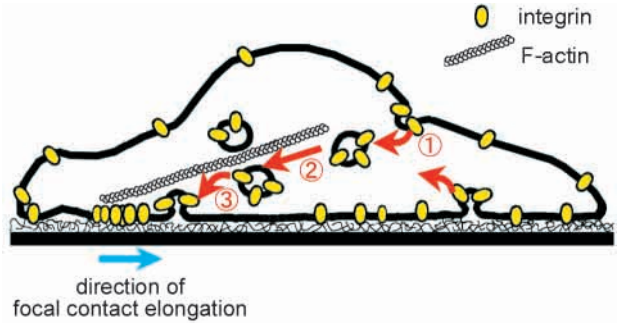

Fig. 8. Hypothetical model of integrin transport and the clustering at FCs. Surface integrins are first internalized, probably by endocytosis (1), and accumulated around the nucleus; this occurs ~30 minutes to 1 hour after plating the cell. Integrins are transported to the ventral side of the cell by an actomyosin-dependent vesicle transport system (2) and are recruited to the tip of extending FC, probably via exocytosis (3) (red arrows show the sequence of these events). The direction of FC elongation in this study was towards the cell centre in most observations (the direction is shown by blue arrow). Elongation ceased when FCs grew to ~7 μm.

The importance of stress fibers for the FC formation has been reported in several studies. Inhibition of FCs formation by cytochalasin D or BDM has been shown in previous studies (Folsom and Sakaguchi, 1997; Folsom and Sakaguchi, 1999) as well as in the present study. We also showed that vesicles containing integrins were associated with stress fibers and that the stress fibers terminated near FCs within 100 nm. Because the vesicle diameter is ~50-300 nm (Heuser, 1980; Orci et al., 1986), the stress-fiber-dependent translocating system could bring vesicles containing integrins to the vicinity of FCs.

Myosin V is associated with punctate structures that are presumably Golgi-derived cytoplasmic vesicles (Espreafico et al., 1992) and/or with small organelles that are colocalized with actin filaments or microtubules (Evans et al., 1997). Under certain conditions, myosin V attached to synaptic vesicles moves along actin filaments (Evans et al., 1998). Inhibition of serine and threonine phosphorylation by H-7 or ML-7 (both block the activity of myosin-light-chain kinase) also resulted in the destruction of actin bundles and FCs (Zamir et al., 2000). The inhibitory action of BDM and ML-9 (and ML-7) on FC formation in this study agrees with the idea that vesicles containing integrins are translocated to FCs in an actomyosin-dependent way (Fig. 8).

The rate of microtubule-based transportation (20-600 μm minute^{-1}) (Vale et al., 1985; Bloom, 1992) was generally higher than that of actomyosin-based transportation (0.1-10 μm minute^{-1}) (Smilenov et al., 1999; Choquet et al., 1997). In the present study, the elongation rate of integrin clusters at FCs was 0.29 μm minute^{-1} and colchicine had no inhibitory effect on the formation of integrin clusters at FCs, again suggesting the presence of actomyosin-dependent translocation of integrins. The integrin-cluster elongation at FCs in this study was towards the cell centre. The actin-dependent transport was reported to be towards the cell centre in many cases (Palecek et al., 1996; Pankov et al., 2000; Zamir et al., 2000). These observations also agree with the idea that elongation of FCs is dependent on the actin fibers.

The mechanisms of integrin incorporation to the extending end of FCs remain unclear. The present observations using FM4-64 strongly suggested that the incorporation of integrin was mediated by exocytosis. Several studies suggested that an actomyosin-based transport step was involved in the exocytosis, because exocytosis at the base of growing microvilli (Fath and Burgess, 1993) in sea urchin eggs was inhibited by BDM (Bi et al., 1997). The inhibitory action of BDM on FC formation in the present study might be due to the inhibition of exocytosis of integrin-containing vesicles in addition to the inhibition of actomyosin-dependent translocation.

The processes of integrin translocation have been studied in migrating cells (Stossel, 1993; Lawson and Maxfield, 1995; Palecek et al., 1996). In these studies, integrins were inserted at the leading edge of migrating cells. However, the observations in the present study showed that FCs were formed independent of cell migration or shape changes. The FCs in HUVECs in the present study elongated towards the center of the cell in a straightforward way (probably along actin fibers). The elongation of FCs does not directly contribute to the extending process of HUVECs. Formations of FCs in HUVECs would strengthen the cell-substrate contact and stabilize the morphology of the cells.

Recent studies (Regen and Horwitz, 1992; Smilenov et al., 1999; Pankov et al., 2000; Zamir et al., 2000) showed the translocation of surface integrins in the fibloblasts. The present study demonstrated that the elongation of integrin cluster ceased when it reached a length of ~7 μm and that the elongated integrin clusters did not move laterally. Therefore, we consider that the FCs we observed here are different from the movable 'extracellular matrix contacts' reported by Pankov et al. (Pankov et al., 2000).

The present study, which focused on the process of FC formation in HUVECs, suggested that the extension of integrins towards the centre is due to the exocytosis of integrin-containing vesicles at FCs. However, the present findings do not exclude the presence of the lateral translocation of surface integrins. The lateral movement of integrins towards the integrin cluster and our model of FC formation are not exclusive; these two mechanisms might both work during FC formation. However, the EpiF (and CLSF) imaging of integrins in the present study showed that most were condensed near the nucleus after the endocytosis of integrins, which will be translocated to FCs, suggesting that most integrins were supplied from the intracellular space in HUVECs. Another possible explanation is that the dynamics of integrin translocation during FC formation in HUVECs might differ from that of the integrin translocation in fibroblasts. The multimode live imaging used in this study will be a powerful tool to clarify the molecular mechanism of FC formation.

This study was partly supported by a Grant-in-Aid for Scientific Research from the Ministry of Education, Science, Sport and Culture of Japan, a grant from the Japan Space Forum, a grant from the future program of the JSPS, and a grant for the object-oriented research from the STA.

REFERENCES

Altankov, G. and Grinnell, F. (1995). Fibronectin receptor internalization and AP-2 complex reorganization in potassium-depleted fibroblasts. *Exp. Cell Res.* **216**, 299-309.

Bi, G. Q., Morris, R. L., Liao G., Alderton, J. M. and Scholey, J. M. (1997). Kinesin- and myosin-driven steps of vesicle recruitment for Ca^{2+}-regulated exocytosis. *J. Cell Biol.* **138**, 999-1008.

Bloom, G. S. (1992). Motor proteins for cytoplasmic microtubules. *Curr. Opin. Cell Biol.* **4**, 66-73.

Bretscher, M. S. (1983). Distribution of receptors for transferrin and low density lipoprotein on the surface of giant HeLa cells. *Proc. Natl. Acad. Sci. USA.* **80**, 454-458.

Bretscher, M. S. (1989). Endocytosis and recycling of the fibronectin receptor in CHO cells. *EMBO J.* **8**, 1341-1348.

Bretscher, M. S. and Thomson, J. N. (1983). Distribution of ferritin receptors and coated pits on giant HeLa cells. *EMBO J.* **2**, 599-603.

Burmeister, J. S., Truskey, G. A. and Reichert, W. M. (1994). Quantitative analysis of variable-angle total internal reflection fluorescence microscopy (VA-TIRFM) of cell/substrate contacts. *J. Microsc.* **173**, 39-51.

Choquet, D., Felsenfeld, D. P. and Sheetz, M. P. (1997). Extracellular matrix rigidity causes strengthening of integrin-cytoskeleton linkages. *Cell* **88**, 39-48.

Cramer, L. P. and Mitchison, T. J. (1995). Myosin is involved in postmitotic cell spreading. *J. Cell Biol.* **131**, 179-189.

Drake, C. J., Davis, L. A. and Little C. D. (1992). Antibodies to β_1-integrins cause alterations of aortic vasculogenesis, in vivo. *Dev. Dyn.* **193**, 83-91.

Ekblom, P., Thesleff, I., Lehto, V. P. and Virtanen, I. (1983). Distribution of the transferrin receptor in normal human fibroblasts and fibrosarcoma cells. *Int. J. Cancer* **31**, 111-117.

Espreafico, E. M., Cheney, R. E., Matteoli, M., Nascimento, A. A. C., De

Camilli, P. V., Larson, R. E. and Mooseker, M. S. (1992). Primary structure and cellular localization of chicken brain myosin-V (p190), an unconventional myosin with calmodulin light chains. *J. Cell Biol.* **119**, 1541-1557.

Evans, L. L., Hammer, J. and Bridgman, P. C. (1997). Subcellular localization of myosin V in nerve growth cones and outgrowth from *dilute-lethal* neurons. *J. Cell Sci.* **110**, 439-449.

Evans, L. L., Lee, A. J., Bridgman, P. C. and Mooseker, M. S. (1998). Vesicle-associated brain myosin-V can be activated to catalyze actin-based transport. *J. Cell Sci.* **111**, 2055-2066.

Fath, K. R. and Burgess, D. R. (1993). Golgi-derived vesicles form developing epithelial cells bind actin filaments and possess myosin-I as a cytoplasmically oriented peripheral membrane protein. *J. Cell Biol.* **120**, 117-127.

Folsom, T. D. and Sakaguchi, D. S. (1997). Characterization of focal adhesion assembly in XR1 glial cells. *Glia* **20**, 348-364.

Folsom, T. D. and Sakaguchi, D. S. (1999). Disruption of actin-myosin interactions results in the inhibition of focal adhesion assembly in *Xenopus* XR1 glial cells. *Glia* **26**, 245-259.

Grimbrone, M. A., Jr (1976). Culture of vascular endothelium. In *Progress in Hemostasis and Thrombosis.* (ed. T. Spaet), pp. 1-28. New York: Grune and Stratton.

Henkel, A. W. and Betz, W. J. (1995). Staurosporine blocks evoked release of FM1-43 but not acetylcholine from frog motor nerve terminals. *J. Neurosci.* **15**, 8246-8258.

Heuser, J. (1980). Three-dimensional visualization of coater vesicle formation in fibroblasts. *J. Cell Biol.* **84**, 560-583.

Hirokawa, N. (1998). Kinesin and dynein superfamily proteins and the mechanism of organelle transport. *Science* **279**, 519-526.

Kumar, C. C. (1998). Signaling by integrin receptors. *Oncogene* **17**, 1365-1373.

LaFlamme, S. E., Akiyama, S. K. and Yamada, K. M. (1992). Regulation of fibronectin receptor distribution. *J. Cell Biol.* **117**, 437-447.

Lawson, M. A. and Maxfield, F. R. (1995). Ca^{2+}- and calcineurin-dependent recycling of an integrin to the front of migrating neutrophils. *Nature* **377**, 75-79.

Luscinskas, F. W. and Lawler, J. (1994). Integrins as dynamic regulators of vascular function. *FASEB J.* **8**, 929-938.

Mallavarapu, A. and Mitchison, T. (1999). Regulated actin cytoskeleton assembly at filopodium tips controls their extension and retraction. *J. Cell Biol.* **146**, 1097-1106.

Mermall, V., Post, P. L. and Mooseker, M. S. (1998). Unconventional myosins in cell movement, membrane traffic, and signal transduction. *Science* **279**, 527-533.

Miyamoto, S., Teramoto, H., Coso, O. A., Gutkind, J. S., Burbelo, P. D., Akiyama, S. K. and Yamada, K. M. (1995). Integrin function: molecular hierarchies of cytoskeletal and signaling molecules. *J. Cell Biol.* **131**, 791-805.

Nakata, T., Terada, S. and Hirokawa, N. (1998). Visualization of the dynamics of synaptic vesicle and plasma membrane proteins in living axons. *J. Cell Biol.* **140**, 659-674.

Oancea, E., Teruel, M. N., Quest, A. F. G. and Meyer, T. (1998). Green fluorescent protein (GFP)-tagged cysteine-rich domains from protein kinase C as fluorescent indicators for diacylglycerol signaling in living cells. *J. Cell Biol.* **140**, 485-498.

Orci, L., Glick, B. S. and Rothman, J. E. (1986). A new type of coated vesicular carrier that appears not to contain clathrin: its possible role in protein transport within the Golgi stack. *Cell* **46**, 171-184.

Palecek, S. P., Schmidt, C. E., Lauffenburger, D. A. and Horwitz, A. F. (1996). Integrin dynamics on the tail region of migrating fibroblasts. *J. Cell Sci.* **109**, 941-952.

Pankov, R., Cukierman, E., Katz, B. Z., Matsumoto, K., Lin, D. C., Lin, S., Hahn, C. and Yamada, K. M. (2000). Integrin dynamics and matrix assembly: tensin-dependent translocation of $\alpha_5\beta_1$ integrins promotes early fibronectin fibrillogenesis. *J. Cell Biol.* **148**, 1075-1090.

Regen, C. M. and Horwitz, A. F. (1992). Dynamics of β_1 integrin-mediated adhesive contacts in motile fibroblasts. *J. Cell Biol.* **119**, 1347-1359.

Ruoslahti, E. (1996). RGD and other recognition sequences for integrins. *Annu. Rev. Cell Dev. Biol.* **12**, 697-715.

Ruoslahti, E. and Engvall, E. (1997). Integrins and vascular extracellular matrix assembly. *J. Clin. Invest.* **99**, 1149-1152.

Saitoh, M., Ishikawa, T., Matsushima, S., Naka, M. and Hidaka, H. (1987). Selective inhibition of catalytic activity of smooth muscle myosin light chain kinase. *J. Biol. Chem.* **262**, 7796-7801.

Schwartz, M., Axelrod, D., Feldman, E. L. and Agranoff, B. W. (1980). Histological localization of binding sites of α-bungarotoxin and of antibodies specific to acetylcholine receptor in goldfish optic nerve and tectum. *Brain Res.* **194**, 171-180.

Sczekan, M. M. and Juliano, R. L. (1990). Internalization of the fibronectin receptor is a constitutive process. *J. Cell Physiol.* **142**, 574-580.

Sheets, E. D., Simson, R. and Jacobson, K. (1995). New insights into membrane dynamics from the analysis of cell surface interactions by physical methods. *Curr. Opin. Cell Biol.* **7**, 707-714.

Smilenov, L. B., Mikhailov, A., Pelham, R. J., Jr, Marcantonio, E. E. and Gundersen, G. G. (1999). Focal adhesion motility revealed in stationary fibroblasts. *Science* **286**, 1172-1174.

Stossel, T. P. (1993). On the crawling of animal cells. *Science* **260,** 1086-1094.

Tatsumi, H., Katayama, Y. and Sokabe, M. (1999). Attachment of growth cones on substrate observed by multi-mode light microscopy. *Neurosci. Res.* **35**, 197-206.

Tawil, N., Wilson, P. and Carbonetto, S. (1993). Integrins in point contacts mediate cell spreading: factors that regulate integrin accumulation in point contacts vs. focal contacts. *J. Cell Biol.* **120**, 261-271.

Vale, R. D., Reese, T. S. and Sheetz, M. P. (1985). Identification of a novel force-generating protein, kinesin, involved in microtubule-based motility. *Cell.* **42**, 39-50.

Zamir, E., Katz, M., Posen, Y., Erez, N., Yamada, K. M., Katz, B. Z., Lin, S., Lin, D. C., Bershadsky, A., Kam, Z. et al. (2000). Dynamics and segregation of cell-matrix adhesions in cultured fibroblasts. *Nat. Cell Biol.* **2**, 191-196.

Zhu, S., Yu, A. W., Hawley, D. and Roy, R. (1986). Frustrated total internal reflection: a demonstration and review. *Am. J. Phys.* **54**, 601-606